Original Article | Neuroimaging and Head & Neck

eISSN 2005-8330
https://doi.org/10.3348/kjr.2020.0816
Korean J Radiol 2021;22(7):1152-1162

Korean Journal of Radiology
KJR

Regional Differences in Blood-Brain Barrier Permeability in Cognitively Normal Elderly Subjects: A Dynamic Contrast-Enhanced MRI-Based Study

Il Heon Ha[1], Changmok Lim[1], Yeahoon Kim[1], Yeonsil Moon[2], Seol-Heui Han[2], Won-Jin Moon[1]

Departments of [1]Radiology and [2]Neurology, Konkuk University Medical Center, Konkuk University School of Medicine, Seoul, Korea

Objective: This study aimed to determine whether there are regional differences in the blood-brain barrier (BBB) permeability of cognitively normal elderly participants and to identify factors influencing BBB permeability with a clinically feasible, 10-minute dynamic contrast-enhanced (DCE) MRI protocol.

Materials and Methods: This IRB-approved prospective study recruited 35 cognitively normal adults (26 women; mean age, 64.5 ± 5.6 years) who underwent DCE T1-weighted imaging. Permeability maps (K_{trans}) were coregistered with masks to calculate the mean regional values. The paired *t* test and Friedman test were used to compare Ktrans between different regions. The relationships between K_{trans} and the factors of age, sex, education, cognition score, vascular risk burden, vascular factors on imaging, and medial temporal lobar atrophy were assessed using Pearson correlation and the Spearman rank test.

Results: The mean permeability rates of the right and left hippocampi, as assessed with automatic segmentation, were 0.529 ± 0.472 and 0.585 ± 0.515 (K_{trans}, x 10^{-3} min^{-1}), respectively. Concerning the deep gray matter, the K_{trans} of the thalamus was significantly greater than those of the putamen and hippocampus (p = 0.007, p = 0.041). Regarding the white matter, the K_{trans} value of the occipital white matter was significantly greater than those of the frontal, cingulate, and temporal white matter (p < 0.0001, p = 0.0007, p = 0.0002). The variations in K_{trans} across brain regions were not related to age, cognitive score, vascular risk burden, vascular risk factors on imaging, or medial temporal lobar atrophy in the study group.

Conclusion: Our study demonstrated regional differences in BBB permeability (K_{trans}) in cognitively normal elderly adults using a clinically acceptable 10-minutes DCE imaging protocol. The regional differences suggest that the integrity of the BBB varies across the brains of cognitively normal elderly adults. We recommend considering regional differences in K_{trans} values when evaluating BBB permeability in patients with neurodegenerative diseases.

Keywords: *Magnetic resonance imaging; Dynamic contrast enhancement; Blood-brain barrier; Permeability; Normal cognition*

INTRODUCTION

Although the pathogenesis of many neurodegenerative and cerebrovascular diseases remains unclear, blood-brain barrier (BBB) breakdown and leakage have been implicated in their mechanism [1-3]; the relationship between BBB permeability and neurodegenerative diseases has thus garnered increasing attention [4]. Studies have reported that BBB breakdown is associated with rapid cognitive decline [5] and contributes to cognitive impairment

Received: March 16, 2020 **Revised:** September 18, 2020 **Accepted:** September 27, 2020
This work was supported by the National Research Foundation of Korea (NRF) grant, funded by the Korean government (MSIP) (no. 2017R1A2B4010634) and no. 2020R1A2C1102896 and a grant from the Korea Health Technology R&D Project through the Korea Health Technology R&D Project through the Korea Health Industry Development Institute (KHIDI), funded by the Ministry of Health & Welfare, Republic of Korea (no. HI18C1038).

Corresponding author: Won-Jin Moon, MD, PhD, Department of Radiology, Konkuk University Medical Center, Konkuk University School of Medicine, 120-1 Neungdong-ro, Gwangjin-gu, Seoul 05030, Korea.
• E-mail: mdmoonwj@kuh.ac.kr

Korean Journal of Radiology
KJR

independent of Alzheimer's disease biomarkers [6,7]. Furthermore, therapeutic strategies have been devised to repair the BBB [8], or radical approaches to open the BBB and allow for the delivery of drugs into the brain have been developed [9]. These methods must be complemented by clinical tools that can elucidate normal values of BBB permeability and thus identify cases of aberrant BBB permeability.

While accuracy and precision are critical to the assessment of BBB permeability in the research of neurodegenerative and small vessel diseases, measurements of BBB permeability can vary with the choice of modality and protocol. Conventionally, the cerebrospinal fluid (CSF)-serum albumin index is used as a measure of BBB breakdown [5,10]. However, CSF-based tests are marred by the invasiveness of CSF sampling and their inability to detect early BBB breakdown due to the large molecular weight of albumin [5,10,11]. Dynamic contrast-enhanced (DCE) MRI with a gadolinium-based contrast agent allows the measurement of subtle BBB permeability changes due to the relatively lower molecular weight of the contrast agent [11,12]. Although DCE MRI is suitable for measuring BBB permeability and leakage, the application of this method to the study of neurodegenerative disease is limited by the lack of standardized protocols and reference values for this method as well as the lack of data on the anatomical distribution of BBB permeability [13,14].

In this study, we aimed to determine whether there are regional differences in the BBB permeability of cognitively normal elderly participants and to identify factors influencing BBB permeability with a clinically feasible, 10-minute DCE MRI protocol.

MATERIALS AND METHODS

Participant Consent

Written consent was obtained from all participants. The study protocol was approved by the Institutional Review Board of the participating institution (IRB No. KUH1140118).

Participant Selection and Clinical Assessment

This prospective study enrolled a total of 35 cognitively normal elderly participants (mean age, 64.5 ± 5.6 years; age range, 54–76 years; nine men) between June 2017 and February 2019. All participants underwent MRI that included protocols for BBB permeability assessment. Out of the 35 subjects, 27 were included as a part of a previous publication [15].

Baseline demographic and clinical characteristics of the participants were assessed, including the current or previous presentation of the following vascular disease risk factors, based on a previous study: diabetes, hypertension, dyslipidemia, history of smoking, cardiovascular disease history, and minor stroke history [16]. The total number of risk factors present in a participant was used as a measure of the vascular risk burden. Global cognitive assessment (Mini-Mental Status Examination [MMSE]) was also conducted. These clinical data were collected within 1–2 months of the MR examination.

We excluded participants suspected of cognitive impairment based on the criteria from the Diagnostic and Statistical Manual of Mental Disorders (4th ed.), National Institute of Neurological and Communicative Disorders and Stroke, and Alzheimer's Disease and Related Disorders Association (NINCDS-ADRDA), and as suggested by Petersen et al. [17] and McKhann et al. [18]). In addition, we excluded participants with other medical conditions associated with dementia-like symptoms, which were assessed using laboratory-based test results.

MRI Sequences

We used a 3T MRI scanner (Skyra, Siemens Healthineers) with a 20-channel phase-array coil to acquire brain images. The following MRI protocols were used: three-dimensional (3D) magnetization-prepared rapid gradient-echo (MPRAGE), 3D fluid-attenuated inversion recovery (FLAIR), and 3D susceptibility-weighted imaging (SWI) sequences.

MRI Protocol (DCE)

The following parameters were used to acquire a coronal 3D DCE sequence of a dynamic series of 60 individual scans: repetition time (TR) = 3.10 ms, echo time (TE) = 1.04 ms, flip angle = 10°, average = 1, field-of-view = 225 x 240 mm, slice thickness = 3 mm, matrix = 180 x 192, voxel size = 1.25 x 1.25 x 3 mm, acquisition time = 10 minutes, time resolution = 10 seconds. We used an acquisition time of 10 minutes in consideration of both patient compliance and mathematical modeling. T1 mapping for the correction of T1 inhomogeneity for kinetic parameter calculations was generated using a pre-contrast T1-weighted gradient-echo series (TR = 3.10 ms, TE = 0.97 ms) with six different flip angles (2–12°). The coronal plane for DCE imaging was perpendicular to the anterior commissure-to-posterior

 https://doi.org/10.3348/kjr.2020.0816

commissure line. A standard dose of gadobutrol (0.1 mmol/kg body weight; Bayer AG) was administered with a 30 mL saline flush, using an automatic injector after the fourth dynamic scan at a flow rate of 2 mL/s. Scans were obtained in the coronal plane because hippocampi and temporal lobes are best assessed by using slices in the coronal plane.

DCE Imaging Analysis

Nordic ICE software (Version 4.1.3; NordicICE) was used by suitably trained neuroimaging research personnel with 3 years of relevant experience, under the supervision of an expert neuroradiologist who was blinded to the clinical information, to process the DCE imaging data and select regions of interest (ROIs) (Fig. 1). 3D T1-volume imaging was used for structural imaging. We used the Patlak model, as it is considered optimal for low-leakage conditions [14,19]. The vascular input function was obtained semi-automatically from the superior sagittal sinus in Nordic ICE. We calculated Ktrans, which indicates the permeability of the surface area product and is equivalent to the volume transfer constant between the plasma and extravascular extracellular space. The quantity leaking per unit time per unit capillary plasma (min^{-1}) was equivalent to 100 x mL/100 g/min.

First, automatic segmentation of the brain regions was performed using the InBrain (https://ww.inbrain.co.kr/; MIDAS Information Technology Co., Ltd.) platform; based on Freesurfer 6.0, InBrain applies deep learning algorithms to the analysis of failure prediction, brain extraction, white matter segmentation, and analysis quality management. As described elsewhere [20,21], the volume of regional brain structures was extracted based on the Desikan Killiany atlas and subcortical atlases. The volumes-of-interest were co-registered to the BBB permeability map to extract the values by using a mutual information-based algorithm to search for an optimal rigid transformation in Nordic ICE. Second, manual ROI analysis was conducted for the following structures: hippocampi, cingulate white matter, frontal white matter, and temporal white matter. We added manual ROI analysis because this additional analysis allowed for easier comparison with several previous studies that had used manual ROI placement for the hippocampi. Structural images (3D T1 MPRAGE) and parametric maps acquired with DCE MRI were co-registered automatically with an algorithm that yielded the most appropriate transformation. The coronal plane at the level

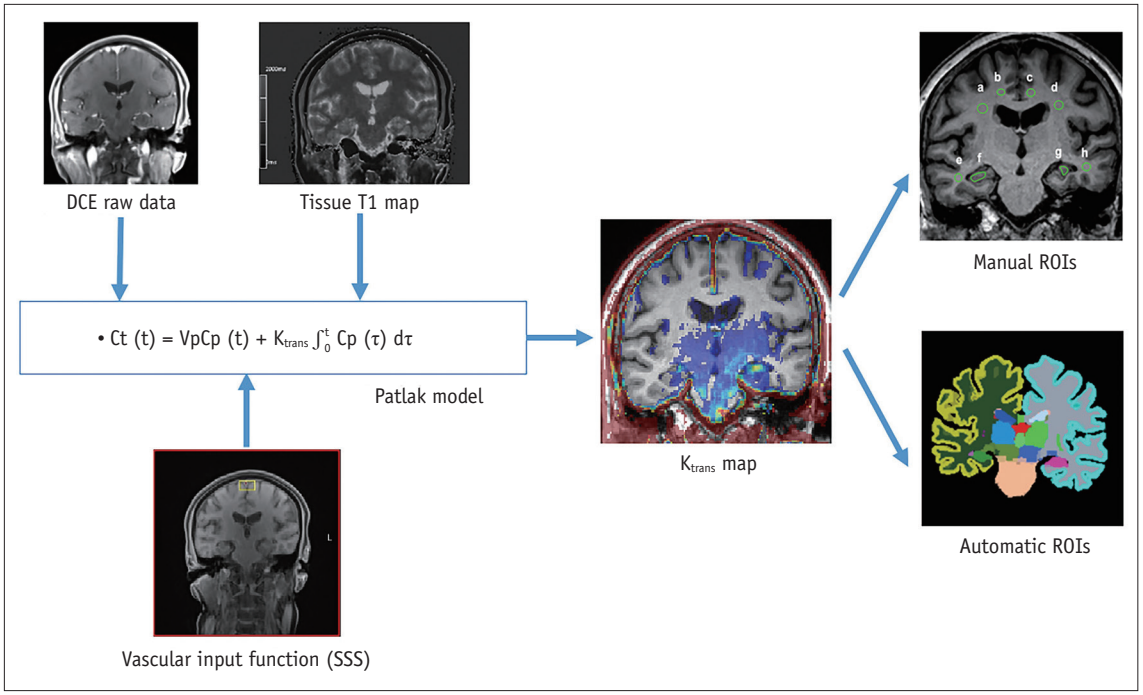

Fig. 1. Analysis process of DCE imaging for K_{trans} measurement. The K_{trans} map was generated from DCE raw data using the Patlak model approach and the SSS as the vascular input function. T1 mapping was obtained and used for accurate calculation of Gd concentration from the Gd relaxivity. Co-registration between the three-dimensional T1-weighted images and K_{trans} map was automatically performed. For automatic ROI analysis, the volumes of interest were extracted from automatic segmentation software. For manual ROI analysis, ovoid or polygonal ROI was placed on the coronal slice at the level of the hippocampal body. DCE = dynamic contrast-enhanced, Gd = gadolinium, ROI = region of interest, SSS = superior sagittal sinus

https://doi.org/10.3348/kjr.2020.0816

Korean Journal of Radiology
KJR

of the interpeduncular cistern of the midbrain was selected for the ROI placement to show the hippocampal body. The polygonal ROIs were drawn manually for the hippocampus on the 3D T1-weighted images while carefully excluding the vessels and CSF before they were transferred to the co-registered K_{trans} map for analysis. Circular ROIs were drawn for white matter regions, carefully excluding potential white matter hypointensities on the 3D T1-weighted images. A neuroradiologist independently performed ROI analysis for the interobserver agreement evaluation of the manual ROI method.

Structural MRI Analysis

Axial-reformatted FLAIR images were used for the visual assessment of vascular risk factors on MRI. A neuroradiologist with 20 years of experience evaluated the images without clinical information. The definition of white matter hyperintensities (WMHs) was based on the Standards for Reporting Vascular Changes in Neuroimaging criteria. WMHs were graded according to the Fazekas scale as deep WMHs (0 = absent; 1 = punctate; 2 = early confluent; 3 = confluent) and periventricular WMHs (0 = absent; 1 = caps or pencil-thin lining; 2 = smooth halo; 3 = irregular WMH, extending into the deep white matter) [22]. The total Fazekas score was calculated by adding the periventricular and deep WMH scores. WMH-positive was defined as a score > 3. Lacunae were defined as small lesions that were hypointense on T1-weighted images, hyperintense on T2-weighted images, and had perilesional halos on FLAIR. Microbleeds were defined as small signal voids that showed blooming artifacts on the SWI images. These findings were recorded as previously described [16,22].

We used the 5-point Scheltens visual rating scale to assess medial temporal lobar atrophy (MTLA) [23,24]. The rating scores ranged from 0 (no atrophy) to 4 (severe atrophy) based on the visual estimation of the choroidal fissure, the width of the temporal horn, and the height of the hippocampal formation.

Statistical Analysis

Statistical analysis was performed using the SPSS (version 25.0 for Windows; IBM Corp.) and GraphPad Prism 8 (GraphPad Software Inc.). A p value < 0.05 was considered to indicate statistical significance. First, the normality of the distribution assumption was tested for all datasets. The paired t test was used to compare the variables of both hemispheres. Comparison of K_{trans} between different regional groups (gray matter nuclei and white matter regions) was performed with the non-parametric Friedman test followed by post-hoc comparison. Spearman's rank correlation for non-parametric variables and Pearson correlation for parametric variables were used to test for a linear correlation between K_{trans} and clinicopathological features (age, education, and cognition scores). We assessed the inter-observer agreement of the measurement using the intraclass correlation coefficient.

RESULTS

The demographic, clinical, and imaging characteristics of the study sample are presented in Table 1.

The permeability rates measured by K_{trans} from each ROI and brain subsection are shown in Tables 2 and 3.

We found no differences in K_{trans} of any of the brain regions studied between the right and left hemispheres (Fig. 2). However, the K_{trans} values of different deep gray matter areas, including the hippocampus, were significantly different (p = 0.003). The right and left thalami showed the highest K_{trans} values among the gray matter regions ($0.693 \pm 0.489 \times 10^{-3}$ min^{-1} and $0.732 \pm 0.512 \times 10^{-3}$ min^{-1}, respectively), while the right and left putamen showed the lowest K_{trans} values ($0.536 \pm 0.456 \times 10^{-3}$ min^{-1} and $0.501 \pm 0.470 \times 10^{-3}$ min^{-1}, respectively). The K_{trans} values in the thalamus were significantly different from those in the putamen and hippocampus (multiplicity-adjusted p = 0.007, p = 0.041). The K_{trans} of white matter regions also differed significantly (p < 0.001). Post-hoc analysis showed higher K_{trans} values in the occipital white matter than in the frontal, cingulate, and temporal white matter structures (multiplicity-adjusted p < 0.001, p < 0.001, p < 0.001).

Table 1. Clinical, Demographic, and Imaging Features of Cognitively Normal Elderly Adults (n = 35)

	Mean ± SD
Age, years	64.5 ± 5.6
Sex, man:woman	9:26
Education, years	12.0 ± 3.7
MMSE score	27.9 ±1.61
White matter hyperintensity (Fazekas) score	1.3 ± 1.2
Lacunae (n)	0
Microbleed (n)	0.5 ± 1.7
MTLA (schelten scale)	0.37 ± 0.49
Vascular risk burden	1.1 ± 0.9

MMSE = Mini-Mental Status Examination, MTLA = medial temporal lobar atrophy, SD = standard deviation

https://doi.org/10.3348/kjr.2020.0816

The mean permeability rates of the right and left hippocampi, as assessed with automatic segmentation, were 0.529 ± 0.472 and 0.585 ± 0.515 (K_{trans}, x 10^{-3} min^{-1}), respectively (Table 2) (Fig. 3). In comparison, the mean permeability rates of the right and left hippocampi, as assessed with the hand-drawn ROI, were 0.808 ± 0.904 and 0.920 ± 1.149 (K_{trans}, x 10^{-3} min^{-1}), respectively.

We found no correlation between the BBB permeability of participants and age, sex, level of education attained, or cognitive scores (MMSE and clinical dementia raging-sum of

Table 2. Distribution of the Mean K_{trans} Values of the Different Brain Regions Defined by the Automated Segmentation Method

	25% Percentile	Median	75% Percentile	Mean	SD	Lower 95% CI of Mean	Upper 95% CI of Mean
Hippocampus							
Hippocampus, right	0.247	0.472	0.670	0.529	0.472	0.381	0.677
Hippocampus, left	0.161	0.515	0.909	0.585	0.515	0.419	0.751
White matter							
CWM, right	0.193	0.278	0.537	0.426	0.730	0.299	0.553
CWM, left	0.169	0.281	0.512	0.408	0.362	0.284	0.553
FWM, right	0.126	0.233	0.443	0.342	0.351	0.222	0.463
FWM, left	0.074	0.198	0.369	0.291	0.287	0.192	0.389
IWM, right	0.196	0.401	0.790	0.555	0.586	0.353	0.756
IWM, left	0.213	0.414	0.900	0.562	0.497	0.391	0.733
TWM, right	0.115	0.200	0.429	0.494	0.809	0.217	0.772
TWM, left	0.110	0.226	0.627	0.501	0.668	0.272	0.731
PWM, right	0.153	0.312	0.534	0.375	0.323	0.264	0.486
PWM, left	0.158	0.464	0.748	0.595	0.609	0.386	0.805
OWM, right	0.248	0.530	0.940	0.911	1.132	0.522	1.300
OWM, left	0.250	0.618	1.339	1.051	1.320	0.597	1.504
Deep gray matter							
CAU, right	0.316	0.523	0.963	0.678	0.596	0.474	0.883
CAU, left	0.303	0.409	0.672	0.514	0.366	0.388	0.640
PAL, right	0.226	0.471	0.807	0.563	0.440	0.412	0.714
PAL, left	0.199	0.463	0.936	0.544	0.402	0.406	0.682
PUT, right	0.249	0.420	0.709	0.536	0.456	0.380	0.693
PUT, left	0.174	0.383	0.598	0.501	0.470	0.339	0.662
THAL, right	0.361	0.614	0.931	0.693	0.489	0.525	0.861
THAL, left	0.343	0.598	1.013	0.732	0.512	0.556	0.908

To aid comparisons with previously reported values, data were presented as the mean and SD, as well as the median and interquartile range, irrespective of the normality of data distribution of the mean K_{trans} values. CAU = caudate nucleus, CI = confidence interval, CWM = cingulate white matter, FWM = frontal white matter, IWM = insular white matter, OWM = occipital white matter, PWM = parietal white matter, SD = standard deviation, TWM = temporal white matter

Table 3. Distribution of the Mean K_{trans} Values of the Different Brain Regions Defined by the Manual Region of Interest Method

	25% Percentile	Median	75% Percentile	Mean	SD	Lower 95% CI of Mean	Upper 95% CI of Mean
HIPP, right	0.156	0.467	1.169	0.808	0.904	0.498	1.119
HIPP, left	0.116	0.501	1.062	0.920	1.149	0.526	1.315
CING, right	0.015	0.333	0.644	0.495	0.651	0.271	0.718
CING, left	0.062	0.246	0.620	0.508	0.762	0.246	0.770
FWM, right	0.037	0.383	1.188	0.727	0.817	0.447	1.008
FWM, left	0.029	0.674	1.186	0.897	1.049	0.536	1.257
TEMP, right	0.000	0.000	0.588	0.419	0.673	0.188	0.651
TEMP, left	0.000	0.043	0.701	0.679	1.218	0.261	1.098

To facilitate comparisons with previously reported values, data were presented as the mean and SD, as well as the median and interquartile range, irrespective of the normality of data distribution of the mean K_{trans} values. CI = confidence interval, CING = cingulate region, FWM = frontal white matter, HIPP = hippocampus, SD = standard deviation, TEMP = temporal region

https://doi.org/10.3348/kjr.2020.0816

Korean Journal of Radiology
KJR

box). BBB permeability did not correlate with the vascular risk burden or analyzed imaging features, including Fazekas score, number of lacunae, presence of microbleed, or MTLA in any brain region.

The inter-rater agreement of the manual ROI placement for K_{trans} ranged from 0.531 [95% confidence interval (CI): 0.078–0.763] (right temporal WM) to 0.878 (95% CI: 0.761–0.938; right cingulate WM). The inter-rater agreements for the manually drawn right and left hippocampi were 0.628 (95% CI: 0.257–0.811) and 0.781 (95% CI: 0.570–0.889), respectively.

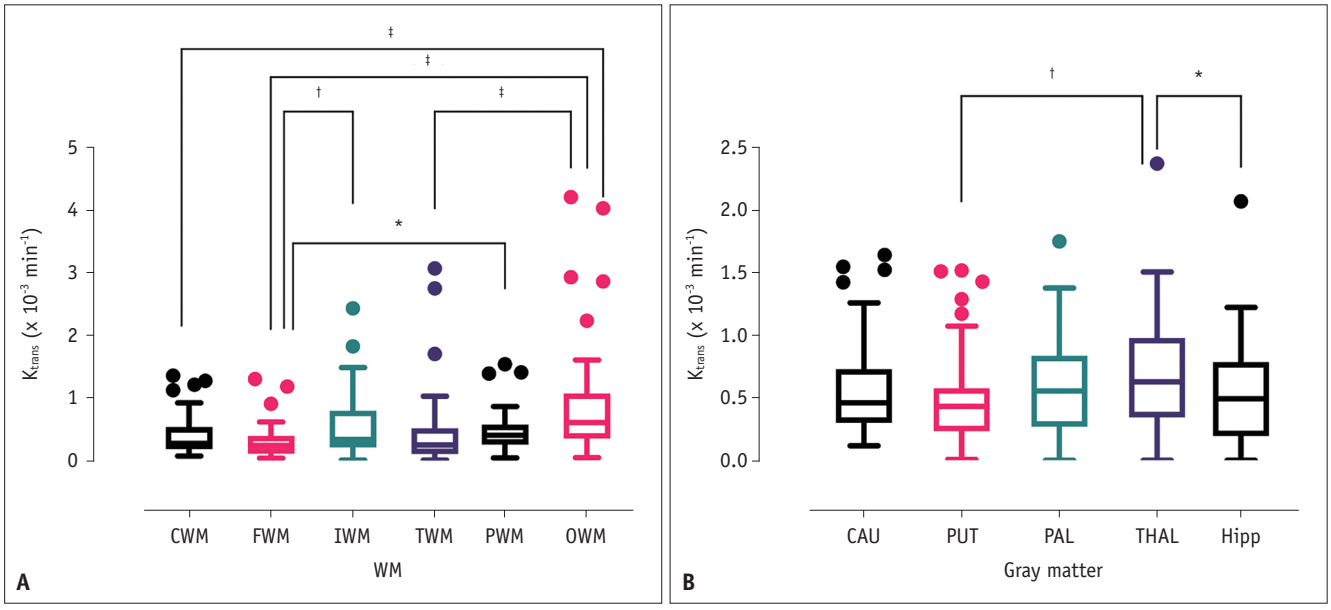

Fig. 2. Box and whisker plot for K_{trans} values in different brain regions.
A. WM regions. **B.** Gray matter regions. All *p* values are multiplicity adjusted values. Denotes **p* < 0.05, †*p* < 0.01, and ‡*p* < 0.001. CAU = caudate nucleus, CWM = cingulate white matter, FWM = frontal white matter, HIPP = hippocampus, IWM = insular white matter, OWM = occipital white matter, PAL = pallidum, PUT = putamen, PWM = parietal white matter, THAL = thalamus, TWM = temporal white matter, WM = white matter

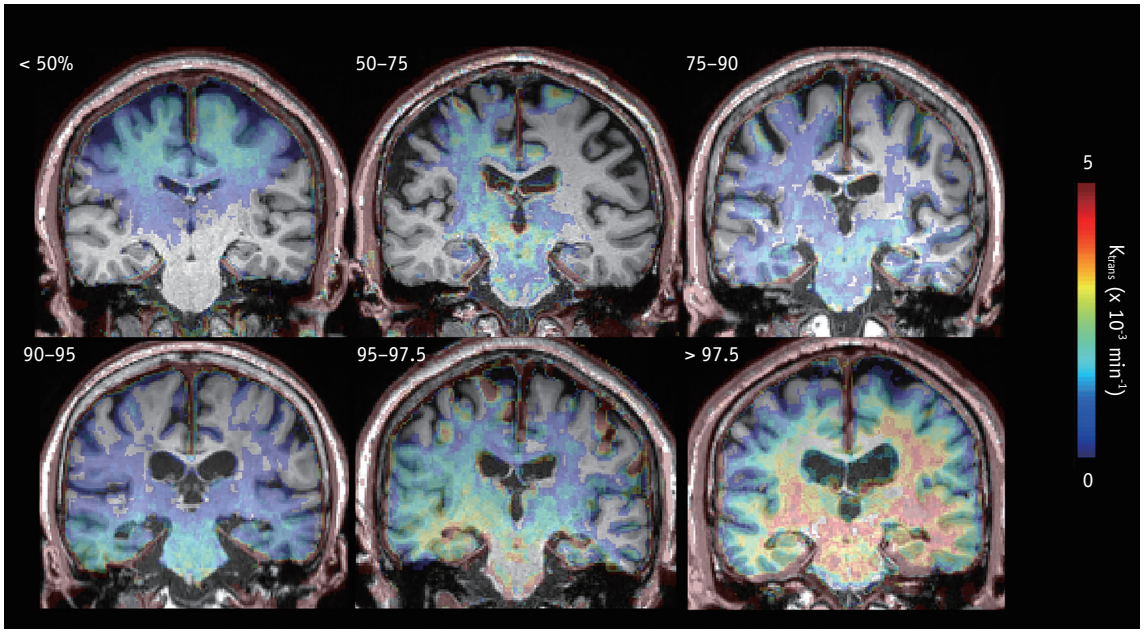

Fig. 3. Representative cases based on the normative distribution of the hippocampal K_{trans} values in cognitively normal elderly adult participants. The presented number denotes the percentile of the K_{trans} values for the hippocampus. Distribution < 50% means that hippocampal K_{trans} of the given subject is below the 50th percentile of the distribution of the hippocampal K_{trans} in 35 normal elderly subjects in our study.

https://doi.org/10.3348/kjr.2020.0816

DISCUSSION

This study presented the regional differences in the K_{trans} values of gray matter nuclei, including the hippocampus and white matter regions of cognitively normal elderly adults (age range, 54–76). Moreover, we have shown that the K_{trans} values of different brain regions were unrelated to age, cognitive score, or vascular risk factors in the study group.

The K_{trans} values reported in previous studies are provided in Table 4. The range of previously reported BBB permeability values varied widely from 2.3 x 10^{-6} min^{-1} to 2.19 x 10^{-3} min^{-1} when converted for measurement unit adjustment [3,6,25-30]. Overall, the K_{trans} values of various brain regions in the present study were similar to or slightly below the values previously reported by Cramer and Larsson [25], Montagne et al. [3], and Yoo et al. [27]. Of the three different models, Cramer and Larsson [25] carefully reported that the Patlak model yielded a normal value of 1 x 10^{-3} min^{-1}, which is close to the presently reported value. In contrast, van de Haar et al. [6], Ivanidze et al. [30], Chi et al. [29], and Kim et al. [28] reported very low values. Furthermore, these previously reported values, even values reported by a single research group, varied within the order of 10 to 1000 [29,30]; in other words, reported values were up to 1000 times higher or lower [27,28].

There are several possible reasons for such discrepancies in K_{trans} values among previous studies. First, different models have been used to obtain K_{trans} values associated with subtle BBB leakage, including the Patlak model and the extended Tofts model [19]. Compared to studies that used the Patlak model [3,25], those that used the extended Tofts model generated significantly smaller K_{trans} values, such as the studies conducted by Chi et al. [29] and Ivanidze et al. [30]. Although the extended Tofts model is favored in brain tumor imaging, its use to assess neurodegenerative disease and/or small vessel disease has not been justified to date [19]. Three previous methodological studies have recommended the Patlak model as the optimal pharmacokinetic model for the DCE imaging analysis of very subtle changes in BBB permeability, such as changes associated with neurodegenerative disease [19,25,31]. The Patlak model is thought to be more accurate in detecting subtle changes in BBB permeability with a high contrast-to-noise ratio for K_{trans} [14,31]. Moreover, in contrast with the extended Tofts model, the Patlak model requires fewer parameters and thus reduces overfitting in low-permeability settings [19].

Second, previous studies used different acquisition schemes. A consensus recommendation regarding acquisition protocols in MRI of BBB permeability has only recently been suggested [14]. However, these previous studies may not have followed this recommendation, as some predate it, while others did not report a detailed acquisition scheme (including information on DCE- and T1-weighted MRI measurements, image preprocessing, selection of vessel input function, model fitting, formulas used, generation of the region and tissue mask, and post-processing and statistical analysis of data) as recommended [32].

Third, K_{trans} values have been reported using different units and are often inadvertently misrepresented. Lack of standardized units can lead to confusion in comparing reported values, particularly when the K_{trans} values are very small. Unit conversion and reporting using consistent units can support comparisons between studies; nevertheless, errors can be introduced in the process. As such, reporting K_{trans} values using standardized units is recommended.

The present study identified significant regional differences in K_{trans} values between brain regions. We found especially higher BBB permeability in the occipital white matter and thalamus than in other white or gray matter regions. The reason for the regional differences in the K_{trans} of the white matter remains unknown. The finding of higher BBB permeability in the thalamus partly agrees with a murine study that observed increased BBB permeability in the dorsal portion of the thalamus and the medial part of the hippocampus [33]. The researchers concluded that higher BBB permeability was associated with proximity to BBB-free areas, such as the subforniceal organs and the choroid plexus [33]. The structural components of the BBB, such as cerebral endothelial cells, pericytes, and astrocytes, are heterogeneously expressed across the central nervous system [34]. Pericyte coverage of brain capillaries differs across the brain, and lower pericyte coverage has been found to correlate with higher BBB permeability [35]. Given the regional diversity of BBB micro-structures and blood flow, it is reasonable to assume that BBB permeability is not uniform throughout the brain even in normal subjects [34].

To compare our findings with those of previous studies, we obtained the K_{trans} values of the hippocampus using two methods: automatic segmentation and the manual ROI approach. Interestingly, although the K_{trans} values of the manually drawn hippocampus were higher than those of other regions generated using the same method, K_{trans} values

https://doi.org/10.3348/kjr.2020.0816

Table 4. Literature Review of Previously Reported Blood-Brain Barrier Permeability Values within the HIPP and/or Other Brain Regions

References	Sample Size (N)	Original Reported Value	Range or SD	Converted Value ($\times 10^{-3}$ min^{-1})	Area	Model	Software	Diagnosis	Age Range (Min - Max)
Cramer and Larsson 2014 [25]	17	0.100 mL/100 g/min		1	FWM and basal ganglia	Patlak	In house	Normal	33 ± 10*
Montagne et al., 2015 [3]	6	1.92 (10^{-3}/min)	0.14	1.92	WM	Patlak	In house	Normal	23–47
	18	2.19 (10^{-3}/min)	0.18	2.19	WM	Patlak	In house	Normal	55–91
	6	0.7 (10^{-3}/min)	0.28	0.7	Thalamus	Patlak	In house	Normal	23–47
	18	0.81 (10^{-3}/min)	0.17	0.81	Thalamus	Patlak	In house	Normal	55–91
van de Haar et al., 2016 [6]	17	1.8 (10^{-4}/min)	1.3	0.18	Cortical gray matter	Patlak	In house	Normal	65–85
Russin et al., 2018 [26]	16	1.74 (10^{-3}/min)	0.07	1.74	Normal brain (in patient with SAH)	Patlak	In house	Aneurysmal SAH	57.6 ± 12.2*
Yoo et al., 2019 [27]	32	0.011 (x 10^{-1}/min)		1.1	HIPP	Toft-Kermode two compartment model	Nordic	Normal	51–67
Kim et al., 2019 [28]	21	2.3 x 10^{-4} mL/100 g/min	1.5–4.8	2.3 x 10^{-3}	HIPP	Patlak	Nordic	Normal	51–87
Chi et al., 2019 [29]	5	0.0008 mL/100 g/min	0.0034	0.008	All brain regions	Extended Toft	Olea	Normal	34.2 ± 10.5*
Ivanidze et al., 2019 [30]	5	0.019 mL/100 g/min	0.049	0.19	HIPP	Extended Toft	Olea	Normal	34.2 ± 10.2*
Present study	35	0.529 (10^{-3}/min)	0.431	0.529	Right HIPP	Patlak	Nordic	Normal	54–76
		0.585 (10^{-3}/min)	0.483	0.585	Left HIPP	Patlak	Nordic		
		0.693 (10^{-3}/min)	0.489	0.693	Right thalamus		Nordic		
		0.732 (10^{-3}/min)	0.512	0.732	Left thalamus	Patlak	Nordic		

*Mean age ± standard deviation. FWM = frontal white matter, HIPP = hippocampus, SAH = subarachnoid hemorrhage, SD = standard deviation, WM = white matter

https://doi.org/10.3348/kjr.2020.0816

Korean Journal of Radiology KJR

of the automatically segmented hippocampus did not differ from those of other regions. The latter result contradicted a previous finding that showed a significantly larger area under the time-intensity curve in the hippocampus than in the other regions [30]. The larger sample size of the present study (35 vs. 6 participants) may account for this discrepancy.

Ivanidze et al. [30] have speculated that the BBB in the hippocampal area is more vulnerable to leakage due to its increased permeability; this is speculated to result from its receipt of blood supply from both the anterior and posterior circulation and its higher neuronal sensitivity to neurodegeneration and aging processes. The difficulty in manually selecting correct ROIs within the hippocampal area while excluding the choroid plexus may explain the conflicting findings in the hippocampus between manual and automated methods. Spatial resolution and slice thickness are other important aspects of correct K_{trans} measurement, as the hippocampal artery and its branches can be included in sections 5 mm thick [32]. This aspect of assessment is important, as contamination with the choroid plexus or inclusion of arteries can result in unexpectedly high K_{trans} values [32]. Inadvertent inclusion of small vessels within the contour of the target anatomy may occur in both manual and automatic methods. Nevertheless, our result of fair to good but not excellent inter-rater agreement on manual ROI analysis implies that automatic segmentation for a specific ROI is favorable over the use of manual ROI placement to avoid unwanted variability in measurements.

In the present study, there was no correlation between K_{trans} values and age among cognitively normal elderly adult participants. Previous studies by Montagne et al. [3] and Nation et al. [7] have shown age-related BBB breakdown in the hippocampus alongside an increase in K_{trans} values in the hippocampal area. These authors speculated that pericyte injury and early degeneration might have resulted in increased BBB permeability [3,36], while the breakdown of the BBB within the hippocampal area during normal aging contributed to cognitive impairment [3,7]. In previous studies, the participants' age range was 23–91 years [3,7]. In the present study, the participants' age range was 54–76 years, as our primary aim was the assessment of elderly adults with normal cognition. Unlike in previous studies, the narrow age range in the present study is unlikely to result in statistically significant differences in permeability of the hippocampal BBB. Nevertheless, an analysis of data from younger participants in future studies might improve our understanding of the relationship between K_{trans} values and age.

The present study found no significant correlations between permeability and vascular risk factors or cognitive scores. This finding might be due to our consideration of cognitively normal elderly adults or due to the independence of BBB permeability from vascular risk factors. Although some of the present study participants appeared to have evidence of small vessel brain disease, its effect on the present findings would have been minimal, as the participants' clinical statuses were normal. Future studies featuring a case-control design are required to confirm our findings.

Considering the practical use of DCE imaging to assess neurodegenerative disease/small vessel disease, it is noteworthy that we obtained BBB permeability values in the normal brain using 10-minute DCE imaging. The recommended acquisition duration is within the 10–30 minutes range [13], and some evidence indicates that an acquisition duration of > 15 minutes is preferred [14]. Although scanning for longer than 10–15 minutes can increase the sensitivity of BBB permeability measurements, it can lead to sharp drops in the contrast-to-noise ratio in high K_{trans} values [31]. Furthermore, longer scanning times require greater patient compliance. The present findings concerning BBB permeability (K_{trans} values) in elderly adult participants might provide a baseline for future clinically feasible and patient-friendly DCE imaging studies that aim to implement DCE imaging acquisition of shorter duration.

The present study has several limitations. First, we only included elderly adult participants with normal cognition. The absence of other groups of different age ranges prevented the definition of the normal regional distribution of BBB permeability. Future studies should conduct comparisons between different age groups and disease populations to validate and expand upon our findings. Second, the present study was a single-center study. Future studies should enroll larger samples to increase the statistical accuracy of the findings. Moreover, external comparisons associated with multicenter studies might be required to obtain generalizable K_{trans} values. Third, the optimal position of the vascular input function remains unclear. Although the vascular input function obtained from the superior sagittal sinus is a good approximation of the arterial input function when using the Patlak model and is believed to yield the most accurate K_{trans} value estimates [14,19], the accurate modeling from the selected vascular

https://doi.org/10.3348/kjr.2020.0816

Korean Journal of Radiology
KJR

input function remains a focus of research. Different approaches, including new imaging sequences with higher temporal stability [37] and deep-learning-based approaches [38], are being tested to overcome this challenge. Finally, although the temporal resolution of our DCE imaging is regarded as adequate [14], it may not be short enough to accurately measure BBB permeability. The accuracy of the K_{trans} values in the modified Tofts and two-compartment models were strongly affected by temporal resolution. However, research indicates that the Patlak model is relatively resistant to modest temporal resolution and yields the best results when combined with fairly long scan times (10–30 minutes) and modest temporal resolution (< 60 seconds) [14,19,31]. Accordingly, we used the Patlak model, which requires the minimum number of parameters to properly fit the data [14,19,25,31]. Hence, although leakage rates can be measured at a low temporal resolution, limiting the scan time for each volume may yield potential benefits [14].

In conclusion, our study demonstrated regional differences in BBB permeability (K_{trans}) in cognitively normal elderly adults using a clinically acceptable 10-min DCE imaging protocol. The regional differences suggest that BBB integrity varies across the normal adult brain. Our study further recommends the consideration of regional differences in K_{trans} values when evaluating BBB permeability in patients with neurodegenerative diseases.

Conflicts of Interest

The authors have no potential conflicts of interest to disclose.

Author Contributions

Conceptualization: Won-Jin Moon. Data curation: Changmok Lim, Yeonsil Moon. Formal analysis: Il Heon Ha, Won-Jin Moon. Funding acquisition: Won-Jin Moon. Investigation: Changmok Lim, Yeahoon Kim, Yeonsil Moon, Won-Jin Moon. Methodology: Changmok Lim, Won-Jin Moon. Project administration: Won-Jin Moon. Resources: Yeonsil Moon, Seol-Heui Han, Won-Jin Moon. Software: Changmok Lim, Yaehoon Kim. Supervision: Won-Jin Moon. Validation: Yeahoon Kim. Visualization: Il Heon Ha, Changmok Lim. Writing—original draft: Il Heon Ha, Won-Jin Moon. Writing—review & editing: all authors.

ORCID iDs

Il Heon Ha
https://orcid.org/0000-0002-3697-6166
Changmok Lim
https://orcid.org/0000-0002-5245-7200
Yeahoon Kim
https://orcid.org/0000-0002-9146-5131
Yeonsil Moon
https://orcid.org/0000-0001-7770-4127
Seol-Heui Han
https://orcid.org/0000-0003-3608-2514
Won-Jin Moon
https://orcid.org/0000-0002-8925-7376

REFERENCES

1. Grinberg LT, Thal DR. Vascular pathology in the aged human brain. *Acta Neuropathol* 2010;119:277-290
2. Wardlaw JM, Doubal FN, Valdes-Hernandez M, Wang X, Chappell FM, Shuler K, et al. Blood-brain barrier permeability and long-term clinical and imaging outcomes in cerebral small vessel disease. *Stroke* 2013;44:525-527
3. Montagne A, Barnes SR, Sweeney MD, Halliday MR, Sagare AP, Zhao Z, et al. Blood-brain barrier breakdown in the aging human hippocampus. *Neuron* 2015;85:296-302
4. Moon WJ. Alzheimer dementia and microvascular pathology: blood-brain barrier permeability imaging. *J Korean Soc Radiol* 2020;81:488-500
5. Bowman GL, Kaye JA, Moore M, Waichunas D, Carlson NE, Quinn JF. Blood-brain barrier impairment in Alzheimer disease: stability and functional significance. *Neurology* 2007;68:1809-1814
6. van de Haar HJ, Burgmans S, Jansen JF, van Osch MJ, van Buchem MA, Muller M, et al. Blood-brain barrier leakage in patients with early Alzheimer disease. *Radiology* 2016;281:527-535
7. Nation DA, Sweeney MD, Montagne A, Sagare AP, D'Orazio LM, Pachicano M, et al. Blood-brain barrier breakdown is an early biomarker of human cognitive dysfunction. *Nat Med* 2019;25:270-276
8. Małkiewicz MA, Szarmach A, Sabisz A, Cubała WJ, Szurowska E, Winklewski PJ. Blood-brain barrier permeability and physical exercise. *J Neuroinflammation* 2019;16:15
9. Lipsman N, Meng Y, Bethune AJ, Huang Y, Lam B, Masellis M, et al. Blood-brain barrier opening in Alzheimer's disease using MR-guided focused ultrasound. *Nat Commun* 2018;9:2336
10. Bowman GL, Dayon L, Kirkland R, Wojcik J, Peyratout G, Severin IC, et al. Blood-brain barrier breakdown, neuroinflammation, and cognitive decline in older adults. *Alzheimers Dement* 2018;14:1640-1650
11. Tofts PS, Kermode AG. Measurement of the blood-brain barrier permeability and leakage space using dynamic MR imaging. 1. Fundamental concepts. *Magn Reson Med* 1991;17:357-367
12. Tofts PS, Brix G, Buckley DL, Evelhoch JL, Henderson E, Knopp MV, et al. Estimating kinetic parameters from dynamic

 https://doi.org/10.3348/kjr.2020.0816

contrast-enhanced T(1)-weighted MRI of a diffusable tracer: standardized quantities and symbols. *J Magn Reson Imaging* 1999;10:223-232
13. Raja R, Rosenberg GA, Caprihan A. MRI measurements of blood-brain barrier function in dementia: a review of recent studies. *Neuropharmacology* 2018;134:259-271
14. Thrippleton MJ, Backes WH, Sourbron S, Ingrisch M, van Osch MJP, Dichgans M, et al. Quantifying blood-brain barrier leakage in small vessel disease: review and consensus recommendations. *Alzheimers Dement* 2019;15:840-858
15. Moon WJ, Lim C, Ha IH, Kim Y, Moon Y, Kim HJ, et al. Hippocampal blood-brain barrier permeability is related to the APOE4 mutation status of elderly individuals without dementia. *J Cereb Blood Flow Metab* 2020 Sep [Epub]. https://doi.org/10.1177/0271678X20952012
16. Park M, Moon Y, Han SH, Kim HK, Moon WJ. Myelin loss in white matter hyperintensities and normal-appearing white matter of cognitively impaired patients: a quantitative synthetic magnetic resonance imaging study. *Eur Radiol* 2019;29:4914-4921
17. Petersen RC, Smith GE, Waring SC, Ivnik RJ, Tangalos EG, Kokmen E. Mild cognitive impairment: clinical characterization and outcome. *Arch Neurol* 1999;56:303-308
18. McKhann G, Drachman D, Folstein M, Katzman R, Price D, Stadlan EM. Clinical diagnosis of Alzheimer's disease: report of the NINCDS-ADRDA Work Group under the auspices of Department of Health and Human Services Task Force on Alzheimer's Disease. *Neurology* 1984;34:939-944
19. Heye AK, Thrippleton MJ, Armitage PA, Valdés Hernández MDC, Makin SD, Glatz A, et al. Tracer kinetic modelling for DCE-MRI quantification of subtle blood-brain barrier permeability. *Neuroimage* 2016;125:446-455
20. Desikan RS, Ségonne F, Fischl B, Quinn BT, Dickerson BC, Blacker D, et al. An automated labeling system for subdividing the human cerebral cortex on MRI scans into gyral based regions of interest. *Neuroimage* 2006;31:968-980
21. Fischl B. FreeSurfer. *Neuroimage* 2012;62:774-781
22. Wardlaw JM, Smith EE, Biessels GJ, Cordonnier C, Fazekas F, Frayne R, et al. Neuroimaging standards for research into small vessel disease and its contribution to ageing and neurodegeneration. *Lancet Neurol* 2013;12:822-838
23. Vermersch P, Leys D, Scheltens P, Barkhof F. Visual rating of hippocampal atrophy: correlation with volumetry. *J Neurol Neurosurg Psychiatry* 1994;57:1015
24. Park M, Moon WJ. Structural MR imaging in the diagnosis of Alzheimer's disease and other neurodegenerative dementia: current imaging approach and future perspectives. *Korean J Radiol* 2016;17:827-845
25. Cramer SP, Larsson HB. Accurate determination of blood-brain barrier permeability using dynamic contrast-enhanced T1-weighted MRI: a simulation and in vivo study on healthy subjects and multiple sclerosis patients. *J Cereb Blood Flow Metab* 2014;34:1655-1665
26. Russin JJ, Montagne A, D'Amore F, He S, Shiroishi MS, Rennert RC, et al. Permeability imaging as a predictor of delayed cerebral ischemia after aneurysmal subarachnoid hemorrhage. *J Cereb Blood Flow Metab* 2018;38:973-979
27. Yoo RE, Choi SH, Oh BM, Do Shin S, Lee EJ, Shin DJ, et al. Quantitative dynamic contrast-enhanced MR imaging shows widespread blood-brain barrier disruption in mild traumatic brain injury patients with post-concussion syndrome. *Eur Radiol* 2019;29:1308-1317
28. Kim YS, Kim M, Choi SH, You SH, Yoo RE, Kang KM, et al. Altered vascular permeability in migraine-associated brain regions: evaluation with dynamic contrast-enhanced MRI. *Radiology* 2019;292:713-720
29. Chi JM, Mackay M, Hoang A, Cheng K, Aranow C, Ivanidze J, et al. Alterations in blood-brain barrier permeability in patients with systemic lupus erythematosus. *AJNR Am J Neuroradiol* 2019;40:470-477
30. Ivanidze J, Mackay M, Hoang A, Chi JM, Cheng K, Aranow C, et al. Dynamic contrast-enhanced MRI reveals unique blood-brain barrier permeability characteristics in the hippocampus in the normal brain. *AJNR Am J Neuroradiol* 2019;40:408-411
31. Barnes SR, Ng TS, Montagne A, Law M, Zlokovic BV, Jacobs RE. Optimal acquisition and modeling parameters for accurate assessment of low Ktrans blood-brain barrier permeability using dynamic contrast-enhanced MRI. *Magn Reson Med* 2016;75:1967-1977
32. Lim CM, Moon WJ. Methodologic concerns on the reported values for assessing permeability of the blood-brain barrier in the hippocampus. *AJNR Am J Neuroradiol* 2019;40:E65-E66
33. Ueno M, Akiguchi I, Hosokawa M, Kotani H, Kanenishi K, Sakamoto H. Blood-brain barrier permeability in the periventricular areas of the normal mouse brain. *Acta Neuropathol* 2000;99:385-392
34. Wilhelm I, Nyúl-Tóth Á, Suciu M, Hermenean A, Krizbai IA. Heterogeneity of the blood-brain barrier. *Tissue Barriers* 2016;4:e1143544
35. Winkler EA, Sengillo JD, Bell RD, Wang J, Zlokovic BV. Blood-spinal cord barrier pericyte reductions contribute to increased capillary permeability. *J Cereb Blood Flow Metab* 2012;32:1841-1852
36. Halliday MR, Rege SV, Ma Q, Zhao Z, Miller CA, Winkler EA, et al. Accelerated pericyte degeneration and blood-brain barrier breakdown in apolipoprotein E4 carriers with Alzheimer's disease. *J Cereb Blood Flow Metab* 2016;36:216-227
37. Lu Y, Ma L, Qin J, Wang Z, Guo J, Zhao Y, et al. The value of GRASP on DCE-MRI for assessing response to neoadjuvant chemotherapy in patients with esophageal cancer. *BMC Cancer* 2019;19:999
38. Ulas C, Das D, Thrippleton MJ, Valdés Hernández MDC, Armitage PA, Makin SD, et al. Convolutional neural networks for direct inference of pharmacokinetic parameters: application to stroke dynamic contrast-enhanced MRI. *Front Neurol* 2019;9:1147